

1 **Title:** Mechanistic links between physiology and spectral reflectance enable pre-visual detection of  
2 oak wilt and drought stress

3

4

5 **Authors:** Gerard Sapes<sup>1,2\*</sup>, Lucy Schroeder<sup>3</sup>, Allison Scott<sup>1</sup>, Isaiah Clark<sup>1</sup>, Jennifer Juzwik<sup>4</sup>, Rebecca  
6 Montgomery<sup>5</sup>, J. Antonio Guzmán Q<sup>1</sup>., Jeannine Cavender-Bares<sup>1\*</sup>.

7

## 8 **Affiliations**

9 <sup>1</sup> Department of Ecology, Evolution, and Behavior, University of Minnesota, Saint Paul,

10 Minnesota 55108, USA

11 <sup>2</sup> Agronomy Department, University of Florida, Gainesville, Florida 32611, USA

12 <sup>3</sup> Department of Plant and Microbial Biology, University of Minnesota, Saint Paul, Minnesota

13 55108, USA

14 <sup>4</sup> Northern Research Station, USDA Forest Service, St. Paul, Minnesota

15 <sup>5</sup> Department of Forest Resources, University of Minnesota, St. Paul, Minnesota 55108, USA

16 \* Corresponding authors

### **Corresponding authors:**

17 Gerard Sapes ([gsapes@ufl.edu](mailto:gsapes@ufl.edu)) and Jeannine Cavender-Bares ([cavender@umn.edu](mailto:cavender@umn.edu))

18 Phone: (406) 207-7955

19 Agronomy Department

20 University of Florida

21 3105 McCarty Hall B, Gainesville, Florida 32603, USA

22

### 23 **ORCID:**

Gerard Sapes: <https://orcid.org/0000-0002-6017-2053>

Lucy Schroeder: <https://orcid.org/0000-0001-8853-8611>

Jennifer Juzwik: <https://orcid.org/0000-0003-0577-7809>

Rebecca Montgomery: <https://orcid.org/0000-0002-4131-1847>

J. Antonio Guzmán Q: <https://orcid.org/0000-0002-0721-148X>

Jeannine Cavender-Bares: <https://orcid.org/0000-0003-3375-9630>

### **Author contribution statement**

J.C.B. Conceived and managed the project. G.S., J.J., R.M. and J.C.B conceived the experimental design and data analysis. G.S., L.S., A.S., I.C., and J.J. collected ground data. A.G.Q. and J.C.B. collected and processed UAV data. G.S. analyzed the data. G.S., L.S., and J.C.B. wrote the manuscript with contributions from J.J., R.M., A.G.Q. J.C.B, J.J., and R.M. obtained funding for this project.

24

25 **Competing Interest Statement:** The authors declare no competing interests.

26

27 **Classification:** Biological Sciences: Environmental Sciences

28

29 **Keywords:** Drought, oak wilt, pre-visual detection, spectral reflectance, remote sensing,  
30 physiology, invasive species, disease, tree mortality.

31

32 This PDF file includes:

33 Main Text

34 Figures 1 to 6

## 35 Abstract

36 Tree mortality due to global change—including range expansion of invasive pests and pathogens—  
37 is a paramount threat to forest ecosystems. Oak forests are among the most prevalent and valuable  
38 ecosystems both ecologically and economically in the United States. There is increasing interest in  
39 monitoring oak decline and death due to both drought and the oak wilt pathogen (*Bretziella*  
40 *fagacearum*). We combined anatomical and ecophysiological measurements with spectroscopy at  
41 leaf, canopy, and airborne levels to enable differentiation of oak wilt and drought, and detection  
42 prior to visible symptom appearance. We performed an outdoor potted experiment with *Quercus*  
43 *rubra* saplings subjected to drought stress and/or artificially inoculated with the pathogen.

44 Models developed from spectral reflectance accurately predicted ecophysiological indicators of oak  
45 wilt and drought decline in both potted and field experiments with naturally grown saplings. Both  
46 oak wilt and drought resulted in blocked water transport through xylem conduits. However, oak wilt  
47 impaired conduits in localized regions of the xylem due to formation of tyloses instead of emboli.  
48 The localized tylose formation resulted in more variable canopy photosynthesis and water content  
49 in diseased trees than drought-stressed ones. Reflectance signatures of plant photosynthesis, water  
50 content and cellular damage detected oak wilt and drought 13 days before visual symptoms  
51 appeared. Our results show that leaf spectral reflectance models predict ecophysiological processes  
52 relevant to detection and differentiation of disease and drought. Coupling spectral models that  
53 detect physiological change with spatial information enhances capacity to differentiate plant stress  
54 types such as oak wilt and drought.

55

## 56 Significance statement

57 The oak wilt pathogen is one of the most destructive threats to oaks in North America. States  
58 invest millions of dollars annually to manage and mitigate its spread. Drought stress is also a  
59 leading cause of tree death and ecosystem collapse in oak dominated forests. Both disturbances  
60 simultaneously impact forests across large spatial scales making early detection and management  
61 extremely challenging. We developed remote sensing tools to detect oak wilt and drought before  
62 visual symptoms appear and differentiate these dual stresses by integrating anatomical,  
63 physiological, and spectroscopic information from cellular to canopy levels. Pre-visual detection of

64 oak wilt when followed by rapid treatment response will reduce incidence, spread and impact of  
65 oak wilt in forest landscapes.

## 66 Introduction

67 Forests provide critical ecosystem services including habitat for organisms, regulation of  
68 climate and air quality, erosion control, and maintenance of global biogeochemical cycles (1).  
69 Multiple global change factors threaten the health of these ecosystems due to rising abiotic and  
70 biotic stress (2). In particular, ongoing climate warming is contributing to increased tree mortality  
71 through compounded heat and drought stress (3), making forests more vulnerable to biotic agents  
72 (4). Increasing human mobility across the globe has heightened vulnerability to biotic stress  
73 through greater exposure to invasive species (5). In North American forests, invasive pests and  
74 pathogens have severely impacted tree species due to increased global warming, drought, and  
75 trade. Protecting forest ecosystems from current and future abiotic and biotic threats is one of the  
76 most pressing challenges of our time (1). Developing methods for accurate and early detection of  
77 tree decline is critical to manage forests and part of an urgent global effort to integrate remote  
78 sensing and ground-based tools to monitor changes in biodiversity for planetary stewardship (6).

79 Oak-dominated forests are the most abundant forest type in the conterminous US and are  
80 critical to maintain ecosystem services in North America, but they face compounding threats of  
81 increasing heat, drought, insect pests, and tree pathogens (7). Local, state, and federal  
82 governments in the US invest hundreds of millions annually to manage and mitigate the impacts of  
83 these threats. Given the ecological and economic importance of oak forests, it is critical to  
84 understand where these forests are at risk of widespread decline due to drought and diseases -  
85 especially as the atmosphere becomes hotter and drier- to manage the spread and impacts of  
86 pathogens. Satisfying this need requires 1) mechanism-based remote sensing tools that can  
87 predict forest health across space, time, and environments; 2) early-detection capabilities to  
88 locate abiotic and biotic stressors rapidly and efficiently; and 3) capacity to distinguish stress types.

89 Among the many invasive pathogens that threaten oak forests, oak wilt caused by  
90 *Bretziella fagacearum* is considered one of the most destructive threats to oaks in the Eastern US  
91 (8). The disease has been documented in 24 eastern states (9) and its intensification is annually  
92 monitored in affected regions (8). The pathogen has severely affected the more vulnerable red oak  
93 lineage (*Quercus* section *Lobatae*) throughout the disease range. Red oak species fail to defend  
94 against and contain the disease once they are infected (10–12). The oak wilt pathogen spreads

95 belowground to neighboring trees through grafted roots and aboveground by insect vectors  
96 (nitidulid beetles and oak bark beetles) that disperse the spores over short to long distances (10).  
97 Long-distance dispersal poses serious challenges to track or predict the advance of oak wilt; thus  
98 early detection of the disease across the landscape is required to limit disease spread. Accurate  
99 detection of oak wilt also requires differentiating its symptoms from those caused by other  
100 stressors such as drought, which can be confused with oak wilt (13). While spectral reflectance has  
101 been used to detect oak wilt in mature trees (14) and to differentiate oak wilt from drought in  
102 greenhouse-grown seedlings (13), pre-visual detection of the disease and differentiation from  
103 drought in an outdoor context has yet to be achieved. In this paper, we link physiology and remote  
104 sensing across spatial scales using proximal and drone-retrieved spectral signals to detect oak wilt  
105 and drought stress before visual symptoms appear and to differentiate both types of stress in an  
106 outdoor potted experiment. We validate the approach in a field experiment on naturally occurring  
107 saplings inoculated with the pathogen.

108

109 Remotely sensed plant spectral reflectance is increasingly used to detect abiotic and biotic  
110 stress in ecosystems at local and landscape scales. Spectral reflectance has been successfully used  
111 to detect disease and insect pest damage such as rapid ohia death, emerald ash borer, bark  
112 beetles, olive decline due to *Xylella fastidiosa*, *Phytophthora*-induced decline of Holm oak as well  
113 as oak wilt (15–23). Drought stress can also be detected spectrally at leaf to landscape scales (24–  
114 29). While studies on the detection of these stress types are increasing, only a handful of studies  
115 show early-detection capacity (i.e., limited symptoms in tree crowns) (26, 30) and even fewer  
116 show pre-visual detection capabilities (19, 31). Underlying this gap is a lack of reflectance datasets  
117 associated with 1) the transition between non-stressed and slightly stressed plants, and 2) the  
118 physiological processes underlying this transition such as photosynthetic decline, turgor loss,  
119 dehydration, cell content leakage, and cell death (4, 32–35). A focus on the onset of plant stress is  
120 therefore key to understanding which spectrally predicted physiological processes might indicate  
121 abiotic and biotic stress before visible symptoms appear. Of the physiological processes associated  
122 with plant stress and mortality, only photosynthetic declines, and dehydration have been  
123 previously linked to spectral features (29, 36). Yet, turgor loss, cell leakage and death can likely be  
124 spectrally detected due to structural and chemical alterations in cells and tissues and used to  
125 inform stress detection at larger scales of canopy, stand, and landscape.

126

127 Studying pre-visual detection of any stress is challenging because the observed data  
128 necessary to construct detection models must meet two requirements. First, it is necessary to  
129 frequently monitor and document changes in visual symptoms throughout the process of stress-  
130 induced plant decline. These data enable us to represent time relative to the first appearance of  
131 visual symptoms instead of time since pathogen inoculation or since the start of an experiment.  
132 Representing timing in terms of symptom appearance is key to identify which physiological  
133 processes are impaired before visual symptoms of stress appear. Biologically-based temporal  
134 variables such as time since visual symptom appearance also reduce plant-to-plant variation that is  
135 not relevant to pre-visual detection by accounting for individual differences in time to symptom  
136 appearance due to plant size, ontogeny, morphology, or environmental heterogeneity (37).  
137 Second, it is necessary to measure the candidate early-detection predictors before, during, and  
138 after the onset of visual symptoms at high frequency and with large sample sizes. These are critical  
139 to capture and accurately model the transition from healthy to declining plant status. An approach  
140 based solely on stress-specific physiological mechanisms might allow for pre-visual detection of  
141 causal stressors such as drought and oak wilt. However, physiological measurements are time  
142 consuming and often destructive, thus precluding high-frequency sampling and large sample sizes.  
143 In contrast, physiological status estimated from rapid and non-destructive observations of spectral  
144 reflectance has the potential to overcome these constraints.

145

146 Oak wilt and drought-stressed oaks show similar progression of symptoms because both  
147 stressors involve impairment of vascular function. Under soil and/or atmospheric drought, water  
148 transport through the xylem is reduced causing declines in turgor pressure, stomatal conductance,  
149 and transpiration rates (38–40). Severe drought triggers embolism formation followed by tissue  
150 dehydration, cell damage, cell content leakage, and eventually plant death (4, 41–43). Infection of  
151 oaks by *B. fagacearum* also reduces water transport through the xylem but does so because of  
152 induced tylose formation rather than embolism. Tyloses are balloon-like defense structures that  
153 irreversibly occlude vessels in response to the presence of the fungus (10, 12). Tyloses can slow  
154 down the spread of the fungus within a tree, but occluded vessels lose function and prevent long-  
155 distance transport of water to the leaves, leading to reduced photosynthesis and transpiration  
156 similar to drought-stressed trees. The overlap in physiological decline processes between oak wilt  
157 and drought makes it challenging to distinguish these two stressors. However, we expect that  
158 differences in the cause of xylem dysfunction (i.e., emboli vs tyloses) and how they are generated

159 (i.e., xylem tension vs fungal infection) provide the mechanistic information necessary to  
160 distinguish between oak wilt and drought.

161

162         The spatial patterning of xylem dysfunction likely differs between oak wilt and drought-  
163 obstructed vessels. Vascular wilts like oak wilt obstruct vessels following infection (44, 45) such  
164 that vessels become obstructed by tyloses as they come into contact with the fungus. As such,  
165 xylem dysfunction develops from the point of pathogen entry inwards, forming clusters of  
166 occluded vessels. Drought stress obstructs vessels by formation of emboli, which form as a  
167 function of vessel vulnerability to tension and tend to occur first in larger vessels (46). Vessel sizes  
168 in ring-porous oaks vary radially from large to small within a given annual growth ring across the  
169 entire cross-section of a stem, such that xylem dysfunction due to drought tends to progress  
170 radially rather than developing locally around a pathogen-colonized area, as in the case of oak wilt.  
171 Spatial patterns of physiological decline in tree canopies likely mirror spatial patterns of xylem  
172 dysfunction because they result from loss of water transport in the vessels that supply the leaves.  
173 Consequently, oak wilt infected trees might show clustered physiological decline in the canopy  
174 with some branches affected while others remain healthy. This would result in high within-canopy  
175 variability in symptoms. In contrast, drought-stressed trees might show more widespread  
176 physiological decline across the canopy (i.e., low within-canopy variability). Because physiological  
177 decline can be correlated with and detected using spectral reflectance data, we test whether  
178 spatially explicit spectral data obtained using low-cost multispectral cameras mounted on  
179 Unoccupied Aerial Vehicles (UAVs) can detect spatial patterns of stress that differentiate oak wilt  
180 and drought. However, the links between both physiological mechanisms and processes and  
181 spectral reflectance across spatial scales necessary to evaluate the potential of multispectral UAVs  
182 as tools to detect drought and oak wilt have yet to be resolved.

183

184 Here, we aimed to 1) determine which physiological processes are impacted as the plant loses  
185 function and which can be estimated through plant spectral reflectance (Fig. 1 O1), 2) identify  
186 which of these spectrally-predicted physiological processes can detect oak wilt and drought before  
187 visual symptoms appear (Fig. 1 O2), and 3) find spectral indices that are compatible with low-cost  
188 multi-spectral UAV sensors that capitalize on physiologically informative wavelengths to detect  
189 and differentiate oak wilt from drought (Fig. 1 O3). We hypothesized that i) processes of plant  
190 dysfunction such as dehydration, cellular death, and cell content leakage can be spectrally

191 detected due to their impacts on tissue structure and chemistry, ii) physiological measurements  
192 related to cell death would detect oak wilt and drought before visible symptoms appear, and iii)  
193 trees infected with the oak wilt pathogen would show higher within-canopy physiological  
194 variability than droughted trees when observed through UAV spectral indices related to cell  
195 damage and death.

## 196 Results

### 197 Physiological progression of oak wilt and drought stress

198 In all treatments of the potted sapling experiment, physiological state remained similar to  
199 the control group (C, Fig. 2 violin plots) values until visual symptoms appeared (Fig. 2, day 0  
200 vertical line). Right before visible symptoms appeared, we observed slight increases in electrolyte  
201 leakage (EL, Fig. 2A) and in loss of rehydration capacity (LRC, Fig. 2F), as well as slight declines in  
202 relative and volumetric water content (RWC and VWC, Fig. 2D-E) in all treatments. In the case of  
203 midday water potential (Fig. 2G), only drought (D) and drought combined with oak wilt (DxOW)  
204 showed slight declines before visible symptoms appeared. Maximum efficiency of photosystem II  
205 ( $F_v/F_m$ , Fig. 2C) showed the earliest decline of all physiological variables measured. However, in  
206 for all variables, confidence intervals were too wide to ascertain pre-visual detection capacity.  
207 After visible symptoms appeared, D, OW, and DxOW treatments showed sharp increases in EL and  
208 LRC and sharp declines in RWC, VWC and water potential (p-value range: 0.022 - <0.001).  
209 Importantly, there were no significant differences in physiological progression between D, OW,  
210 and DxOW treatments.

### 211 Spectral reflectance progression of oak wilt and drought stress

212 In the potted sapling experiment, we observed increasingly significant shifts across several  
213 wavelength regions of the canopy spectra as oak wilt and drought stress visual symptoms  
214 increased in severity (Fig. 3A & B, Appendix S6). The first shifts in spectral reflectance appeared in  
215 canopies 33 days after imposing treatments. In OW trees, canopy spectral reflectance first  
216 increased at 1400-1500 nm within the short-wave infrared (SWIR) ( $p < 0.01$ ). The red edge region  
217 declined at 700-750 nm at 48 days ( $p < 0.01$ ). By day 62, nearly the full spectral range was different  
218 than controls except for the green region of the visible range (VIS), some areas of the red edge,  
219 and SWIR wavelengths around 1600 nm. In D trees, canopy spectral reflectance first decreased at  
220 ca. 1150 nm of the NIR ( $p < 0.01$ ) and those detected in OW by day 33. After 48 days, significant

221 wavelengths were found in the blue and red VIS regions, between 1000-1270 nm, 1400-1500 nm,  
222 and 1950-2200 nm ( $p < 0.01$ ). After 62 days, nearly the full spectral range was different like in the  
223 case of OW ( $p < 0.01$ ). DxOW also manifested changes at 33 days; significant wavelengths were a  
224 combination of the first wavelengths detected in OW and D trees, plus a region at 1600-1750 nm  
225 ( $p < 0.01$ ). By day 48, DxOW trees showed significant wavelengths across the whole spectral range  
226 ( $p < 0.01$ ) similar in direction and magnitude to those observed in OW trees by day 62.

227 Shifts in leaf spectral reflectance lagged those of canopy reflectance. Although the shape  
228 of the spectra was already changing by 33 days, we did not observe significant differences until 62  
229 days because we set our alpha threshold at 0.01. At 62 days, we observed increases in the VIS  
230 range, declines in reflectance across and beyond the VNIR range (750-1300 nm), and increases at  
231 the SWIR range ( $p < 0.01$ ) of the spectra (Fig. 3-IV-A). D leaves first showed increased reflectance  
232 at the red region of the VIS ( $p < 0.01$ ) by day 33. The blue and the 750 nm regions increased and  
233 decreased ( $p < 0.01$ ) respectively, and reflectance at the SWIR water bands increased ( $p < 0.01$ ) by  
234 day 48. Nearly the full range of the spectra of D leaves was different than controls by day 62.  
235 DxOW leaves went from no difference from controls to suddenly being the most spectrally  
236 different, with nearly all regions of the spectra showing significant differences by day 62 ( $p < 0.01$ ).

### 237 Predicting physiology from spectra

238 PLSR models based on leaf spectral reflectance predicted relative and volumetric water  
239 content (RMSEP = 11.47%, 10.76% respectively), loss of rehydration capacity and electrolyte  
240 leakage ((RMSEP = 11.98%, 13.09% respectively), water potential (RMSEP = 19.77%), and  
241 maximum efficiency of photosystem II (RMSEP = 16.16%) both when all trees were used and when  
242 controls were excluded (Appendix S7). When applied to data from the outdoor potted experiment  
243 not used to train models (cross-validation), measured vs predicted plots showed similar slopes  
244 among treatments (Fig. 4 A, C, E, G) which indicated that physiological status was predicted with  
245 similar bias regardless of the type of stress. When models were independently validated with  
246 measurements from a natural population of red oaks infected inoculated with *B. fagacearum* at  
247 Cedar Creek, spectrally predicted VWC and Fv/Fm nicely tracked the measured values both in  
248 control and oak wilt diseased trees (Fig. 4 B, D). VWC and Fv/Fm of the diseased trees diverged  
249 from controls (no overlap in confidence intervals) before visible symptoms appeared (day 22 after  
250 inoculation) in both measured and spectra-predicted values. Spectra-predicted VWC and Fv/Fm  
251 also tracked a slight recovery in VWC and Fv/Fm that occurred after a rain pulse around day 70

252 after inoculation. Based on the success of VWC and Fv/Fm spectral models to predict measured  
253 values at Cedar Creek, we decided to apply two other spectral models (LRC and EL) that showed  
254 good cross-validation performance to the Cedar Creek dataset. While we did not measure LRC and  
255 EL at Cedar Creek to validate predictions, spectrally predicted LRC and EL in these plants showed  
256 clearly distinct patterns between oak wilt diseased and control trees (Fig. 4 F, H).

257 Distinguishing oak wilt from drought stress in xylem and canopies

258 Trees infected with *B. fagacearum* that showed no visual symptoms by the end of the  
259 experiment (asymptomatic) retained some of their xylem functional, but less than controls ( $p <$   
260  $0.05$ ), whereas symptomatic trees lost all their functional xylem ( $p < 0.001$ , Appendix S9). Xylem  
261 occluded by tyloses could not be removed by flushing, whereas embolisms caused by drought  
262 could be flushed ( $p < 0.05$ , Fig. 5C), differentiating hydraulic dysfunction caused by drought from  
263 that caused by oak wilt. Hydraulic dysfunction associated with oak wilt showed a spatial pattern  
264 typical of a pathogen that is carried in the transpiration stream from a point of infection (or  
265 artificial inoculation) toward contiguous sections of the xylem; whereas drought affected trees  
266 showed no spatial pattern ( $p < 0.001$ , Fig. 5C). Trees subjected to both drought and oak wilt  
267 (DxOW) exhibited xylem occlusion levels intermediate to those of D and OW trees and were not  
268 significantly different from either group ( $p > 0.05$ , Fig. 5C, Appendix S9). These DxOW trees  
269 exhibited both contiguous and non-contiguous hydraulic dysfunction, covering the range of  
270 responses observed in both D and OW trees. However, their spatial pattern was statistically most  
271 similar to that of D trees.

272 The average canopy pixel value from the UAV sensor for the Re-normalized Difference  
273 Vegetation Index (RDVI), which uses key wavelengths identified by our spectrally predicted  
274 physiological models (Appendix S7), declined in OW, D, and DxOW trees as drought and oak wilt  
275 progressed (Fig. 3C-F, I-IV). However, the within-canopy standard deviation in RDVI increased in  
276 OW trees relative to D trees as the disease progressed and visible symptoms appeared ( $p = 0.02$ ,  
277 Fig. 5B).

278 Detecting oak wilt and drought stress before visible symptoms appear

279 Bayesian segmented regressions identified an inflection point corresponding to the day at  
280 which spectrally predicted physiology started to change in response to stress (Fig. 6A). Fv/Fm had  
281 the highest pre-visual detection capacity, showing spectrally predicted Fv/Fm declines in D, OW,  
282 and DxOW treatments at about 11, 12, and 6 days (respectively), but up to 27, 24, and 12 days

283 (respectively) before visible symptoms appeared (Fig. 6B, Appendix S10). LRC could also detect  
284 drought and oak wilt before visible symptoms appeared. On average, increases in LRC could be  
285 spectrally detected in D, OW, and DxOW treatments about 8, 6, and 5 days, but up to 15, 11, and 9  
286 days (respectively), before visible symptoms appeared. Water potential, VWC, RWC, and EL could  
287 pre-visually detect D and DxOW stress within similar timeframes as LRC. However, in trees of the  
288 OW treatment, their detection threshold was not significantly different from the day of visible  
289 symptom appearance.

## 290 Discussion

291 A long-standing challenge in remote sensing of plant stress is to detect and differentiate  
292 stress types by causal factor early enough to improve efficacy of local site treatments for disease  
293 management. Our results show that leaf spectral reflectance can detect oak wilt and drought  
294 approximately two weeks before visual symptoms appear and can differentiate the two stressors.  
295 Accurately differentiating oak wilt symptoms from drought-induced stress requires coupling leaf  
296 spectra to the physiological processes and mechanisms underpinning each causal factor to identify  
297 wavelengths associated with early physiological decline. We find that spatial patterns of spectral  
298 indices sensitive to oak wilt and drought can help differentiate these stresses using relatively low-  
299 cost multi-spectral UAV sensors. Our results highlight the importance of mechanistically linking  
300 characteristics derived from remote sensing to physiological processes to improve monitoring of  
301 forest health.

302 Reflectance-based physiological models detect oak wilt and drought

303 Physiological processes linked to photosynthesis, dehydration, and cell death can be  
304 predicted from leaf spectral reflectance. Declining turgor and stomatal closure are the first  
305 processes to occur in oak wilt and drought-stressed oak seedlings (13). In trees infected with *B.*  
306 *fagacearum*, these changes result from clogged conduits (Fig. 5C) (10). In drought-stressed trees,  
307 decreased turgor and closure of stomata occur due to decreasing water potentials triggered by  
308 water deficit (4). Prolonged stomatal closure eventually impacts chlorophyll concentrations,  
309 manifested in leaf spectra as an increase in reflectance at red and blue wavelengths (47). Increases  
310 in reflectance at red and blue wavelengths are among the first to occur in oak wilt and drought  
311 stressed trees (Fig. 3A, Appendix S6) and are a strong predictor of physiological processes linked to  
312 photosynthesis such as maximum quantum efficiency of Photosystem II (Fv/Fm) (Appendix S8).  
313 After photosynthetic inhibition and turgor loss, leaves continue to dehydrate and start to

314 experience permanent and irreparable damage to cell walls due to cellular collapse (i.e.,  
315 cytorrhysis, which causes loss of rehydration capacity) (42). Cellular contents leak through  
316 degraded membranes, and cells die (Appendix S8). Dehydration, cytorrhysis, and cell leakage all  
317 increased leaf reflectance across wavelengths that are absorbed by water and decreased  
318 reflectance across wavelengths sensitive to changes in cell mesophyll structure and pigment  
319 content (Appendix S6 & S8). Cytorrhysis and cell leakage are processes that occur nearly  
320 simultaneously due to dehydration (42). As such, they occur at similar times relative to the onset  
321 of visible symptoms for both oak wilt and drought (Fig. 2).

322 The reflectance-based models that we built to predict these physiological processes were trained  
323 in a controlled experimental setup with one species (*Quercus rubra*). Yet, they detected  
324 physiological stress caused by oak wilt in the field despite the variability inherent to natural  
325 communities with mixed species – two red oak species (*Q. rubra* and *Q. ellipsoidalis*) in our case –  
326 and uneven ages (Fig. 4). Predicted vs measured values showed variability at intermediate values  
327 of the measured physiological range. This could occur because spectral reflectance is not a perfect  
328 predictor of physiological characteristics or due to within-leaf variability in physiology and spectra.  
329 Within-leaf variability is captured by the small field of view of the fiber optic but not by  
330 physiological measurements that are measured at the whole leaf level. Covering a wide range of  
331 physiological values during model training ensured that measured vs predicted slopes remained  
332 close to the 1:1 line and intermediate values could be accurately predicted. Accordingly,  
333 spectrally-predicted physiology at the Cedar Creek experiment tracked measured physiology even  
334 at intermediate values of the measured range of the testing data (Fig. 4B,D). We were also able to  
335 distinguish trees infected with *B. fagacearum* from healthy trees based on LRC and EL models  
336 despite having no physiological observations for these variables in the field (Fig. 4F,H). These  
337 results suggest that reflectance-based physiological models provide lower risk of faulty  
338 extrapolation and higher chance of success than models that do not have a physiological basis  
339 when applied to new locations, periods, or species. Our findings indicate that spectroscopic  
340 models of plant stress that are grounded in the physiological mechanisms and processes that  
341 plants undergo during oak wilt disease progression and drought can produce general insights.

342 Oak wilt and drought can be detected a week before visual symptoms appear

343         While all spectrally predicted physiological processes were able to detect drought stress  
344 before visual symptoms appeared, only Fv/Fm and loss of rehydration capacity (LRC) could do so

345 for oak wilt (Fig. 6). Fv/Fm and LRC can detect oak wilt and drought approximately one week  
346 before leaves exhibit visual symptoms. This is likely because they are associated with early signs of  
347 stress, such as photosynthetic declines and turgor loss (48, 49). While only two spectrally  
348 predicted physiological processes could detect oak wilt before visual symptoms appeared, all of  
349 them could detect oak wilt disease within 3 days after the first leaf showed visual symptoms in a  
350 tree (Fig. 6). Landscape detection of oak wilt by ground detection surveys (GDS) conducted by  
351 personnel trained to recognize visual crown symptoms and other site clues are labor intensive,  
352 slow, and based on advanced crown symptoms (e.g., > 30 % of crown affected) (10). Close  
353 examination of suspect trees by GDS is required to differentiate diseased and droughted trees.  
354 Aerial detection surveys monitor landscapes more quickly, but ground-truthing of suspect sites is  
355 also required if both droughted and diseased trees are present because they cannot be  
356 distinguished from the air. Management strategies can fail to contain oak wilt because the disease  
357 often has already spread via insect vectors to nearby trees by the time the symptomatic trees are  
358 correctly diagnosed and sites treated (10). Our results suggest that oak wilt and drought could be  
359 detected much earlier using spectral reflectance data from remote sensing platforms. Survey  
360 crews could monitor larger areas with fewer people and quickly respond with treatments before  
361 the pathogen has a chance to spread. Pre-visual detection via spectra could also improve methods  
362 aimed at stopping pathogen spread through inter-tree root grafts. For instance, pre-visual  
363 detection could improve delineation of outer perimeter lines of oak wilt centers and surrounding  
364 buffers which are currently based on experience or statistical models (50) and that sometimes  
365 miss asymptomatic but already infected trees. Currently, UAVs equipped with RGB sensors are  
366 used to detect single trees exhibiting oak wilt symptoms in forest compartments in Menominee  
367 County, WI, USA, managed by Menominee Tribal Enterprises foresters. A rapid response  
368 treatment has been devised to prevent spread of the pathogen downward into the root systems  
369 and then to adjacent trees. The treatment involves making two stem girdling cuts 15 to 25 cm  
370 apart into the outer xylem of the lower main stem of a tree exhibiting incipient wilt and applying  
371 liquid herbicide to the fresh cuts. Low-cost multispectral UAVs like ours would maximize the time  
372 window during which these treatments are effective. In terms of drought, early detection can  
373 greatly improve our ability to forecast and manage forest health under future drier conditions and,  
374 for instance, take action to increase forest defenses against biotic agents or reduce fire risk  
375 resulting from higher flammability of droughted stems.

376 Distinguishing oak wilt from drought requires combining physiology and spectral  
377 reflectance

378         The leaf-level physiological processes that trees experience as they develop oak wilt and  
379 drought symptoms (Fig. 2) are similar because the causal agent is the same: a loss of hydraulic  
380 conductivity in the xylem (Fig. 5C). As such, leaf-level physiology alone cannot distinguish oak wilt  
381 from drought stress. However, how loss of hydraulic conductivity manifests spatially through the  
382 xylem differs between oak wilt and drought-stressed trees (Fig. 5C). Loss of hydraulic conductivity  
383 in trees infected with oak wilt results in a clustered spatial pattern of xylem dysfunction that does  
384 not occur in drought stressed trees. It is therefore possible to distinguish between oak wilt and  
385 drought using xylem staining techniques, but this approach is impractical for large-scale  
386 assessments. Yet, the spatial differences in xylem dysfunction provide the causal physiological  
387 mechanism that allows differentiation of both stressors at larger scales. Because branches in the  
388 canopy are connected to different sets of conduits at the base of the stem, trees at early stages of  
389 oak wilt crown symptom development show photosynthetic decline, dehydration, and cell death  
390 only in the subset of branches connected to occluded xylem vessels (Fig. 3C). This pattern  
391 generates large variability in physiological status across the canopy as symptoms develop (Fig. 5B).  
392 By coupling the physiological processes to spectral reflectance data, we identified wavelengths  
393 sensitive to these processes and used them to select spectral indices observable with low-cost  
394 UAVs such as the RDVI index; shown to be amongst the most sensitive to oak wilt (14). The  
395 wavelengths 900 and 690 nm used in this index are linked to photosynthetic activity and leaf  
396 structural integrity (51) -confirmed by our PLSR models (Appendix S8)-, which explains the  
397 sensitivity of this index. This trans-disciplinary approach enabled us to detect spatial variability in  
398 physiological status and to distinguish trees at early stages of oak wilt development from drought-  
399 stressed trees (Fig. 5B, Fig. 3C,D). Our results show that it is critical to consider spatial patterns as  
400 part of a mechanistic approach at all scales (i.e., tissue, organ, and individual). Considering xylem,  
401 leaf, and canopy patterns together was essential for distinguishing oak wilt from drought. Spatial  
402 patterns are also important for detecting oak wilt at both tree and stand levels because it reduces  
403 misclassification and allows detection of oak wilt pockets (14). Because oak wilt manifests similarly  
404 across the extant range of red oaks (*Quercus* section *Lobatae*) (52), we are hopeful that both the  
405 patterns observed in this study and our approach will be broadly applicable.

## 406 Conclusions

407 Throughout the decades-long history of remote sensing, scientists have aspired to monitor  
408 plant stress from the skies with the click of a button (53) —but that day has been slow to arrive.  
409 One reason may be that remote sensing approaches frequently lack the mechanistic basis to be  
410 generalized across space, time, and biological systems (54). The field of plant ecophysiology has  
411 long claimed to provide a solid mechanistic foundation that could be used to monitor the severity  
412 of plant stress in a general way (55). However, collecting large-scale ecophysiological data at  
413 temporal and spatial resolution needed to monitor plant stress across landscapes is impractical.  
414 Our study shows that combining both disciplines, into what could be called spectral ecophysiology,  
415 provides the best of both worlds. In our case, it enabled early detection and differentiation of the  
416 biotic and abiotic stressors that cause oak wilt and drought. Ecophysiology informs which plant  
417 processes should be predicted from remotely sensed spectral reflectance. Remote sensing enables  
418 high-throughput, spatially-explicit estimates of such processes. Spectrally-predicted ecophysiology  
419 and spectral indices grounded in ecophysiology are tied to fundamental biology. They are  
420 therefore likely to generalize better than reflectance signals that are not connected to mechanism.  
421 We hope that our research motivates future studies to explore the linkages between  
422 ecophysiology and spectral reflectance; to discern what can—and cannot—be measured, when,  
423 and in which plant systems.

## 424 Methods

### 425 Experimental design

426 In the spring of 2019 and 2021, we conducted two experiments: 1) a field experiment with  
427 naturally-regenerated red oak saplings artificially inoculated with *B. fagacearum* at the Cedar  
428 Creek Ecosystem Science Reserve (45.396 N, 93.183 W, Appendix S1) and 2) an outdoor potted  
429 experiment with *Quercus rubra* in which we applied a drought treatment and an oak wilt  
430 treatment (artificially inoculated with the pathogen) in a full-factorial design outside the Plant  
431 Growth Facilities of the University of Minnesota St. Paul Campus (44.988 N, 93.177 W).

432 For the Cedar Creek experiment, we selected forty naturally growing *Q. ellipsoidalis* and *Q.*  
433 *rubra* saplings with fully developed leaves. We chose a mixture of species because they are  
434 difficult to differentiate as juveniles and freely introgress. Both species are equally susceptible to  
435 oak wilt. Trees ranged from 63 to 240 cm tall with an average height of 134 cm, and basal  
436 diameters at groundline ranged from 1.2 to 5.4 cm with an average diameter of 2.8 cm. On June

437 27<sup>th</sup> 2019, we inoculated half of the trees (OW treatment) with *B. fagacearum* introduced as 1 mL  
438 of a homogenized aqueous spore suspension ( $2.1 \times 10^5$  spores  $\times$  mL<sup>-1</sup>) pipetted into a single freshly  
439 drilled hole (1-mm diameter  $\times$  4 cm in radial depth) placed 4 cm above the root collar. Sterile moist  
440 cotton was then placed over the wound and affixed to the stem with parafilm. The rest of the  
441 trees remained untreated as a control treatment. We tracked physiological and spectral changes in  
442 OW and C trees at 14, 25, 42, 62, and 74 days after inoculation. At each sampling date, we  
443 randomly selected five OW trees along with their nearest five control trees. This sampling scheme  
444 minimized spatial variation unrelated to the treatments.

445 In the outdoor potted experiment at the Plant Growth Facilities, we planted 100 bare-root  
446 saplings in pots. Trees ranged from 27 to 133 cm tall with an average height of 96 cm, and basal  
447 diameters calculated from stem perimeter at groundline ranged from 0.64 to 1.81 cm with an  
448 average diameter of 1.00 cm. On April 13-14, 2021, we replanted the dormant trees in 9.63L cone-  
449 shaped pots white-painted to prevent overheating of the root system and with a 2:1 mix of potting  
450 soil and sand. Trees were placed outside where they subsequently flushed prior to application of  
451 treatments. On July 15<sup>th</sup>, we inoculated half of the trees with the same inoculum concentration  
452 used at Cedar Creek. A small bark flap was cut, ring of putty applied below the cut, an aqueous  
453 suspension of inoculum introduced, and the wound covered as previously described. Half of the *B.*  
454 *fagacearum* inoculated trees (OW) and half of the non-inoculated trees were covered with white  
455 cling film around the base to exclude rain and induce drought. Thus, we had four treatments in a  
456 full factorial design: control (C), drought (D), oak wilt (OW), and drought and oak wilt (DxOW).  
457 Treatments were randomly distributed, and trees were evenly spaced (ca. 0.5 m apart). We  
458 tracked physiological changes in five different, randomly selected OW, D, DxOW, and C trees after  
459 inoculation on a weekly basis. Additionally, full-range spectral reflectance (400 – 2400 nm) at both  
460 leaf and canopy levels were measured in every tree on each of the sampling days. Finally, we  
461 tracked canopy visual appearance every 3 days to identify the date on which each tree first  
462 showed visible symptoms of stress.

#### 463 Sampling procedure

464 In both experiments, we assessed the canopy of each tree to record the proportion of  
465 leaves at each of four symptomatic stages to identify leaves at different symptomatic stages  
466 (green, drooping and discolored; drooping and brown edges; and entirely brown and dry). We  
467 selected representative leaves of each stage present in the target trees for physiological and  
468 spectral measurements (see below). This sampling approach was designed to ensure strong

469 representation of the entire range of observed variation in spectra and physiology, which helps  
470 train robust spectral models. For each leaf type present, we chose a sun leaf and dark-acclimated  
471 it overnight using a light-blocking clip (Hansatech, PP Systems). The following day, we took the  
472 fluorescence in the morning and spectral measurements around midday in the selected leaves. We  
473 collected leaves and placed them in Ziploc bags containing a moist paper towel partially covered in  
474 aluminum foil to prevent desiccation without introducing external moisture into the leaf by  
475 contact with the towel (56). Leaves were then placed in a cooler and transported to the lab to  
476 measure their water status.

477 Chlorophyll fluorescence, leaf and canopy hyperspectral, and UAV multispectral reflectance  
478       In the morning (9:00) of each sampling date and for both experiments, we measured  
479 Fv/Fm using a Hansatech chlorophyll fluorometer (PP Systems, Narborough, UK) under dark-  
480 acclimated conditions. Fv/Fm is a measure of maximum photosynthetic quantum efficiency under  
481 dark acclimated conditions and can be used to indicate leaf tissue vitality and stress (32, 57).  
482 Around midday (11:00 to 13:00), we measured full-range leaf spectral reflectance (400 to 2400  
483 nm) using a PSR+ 3500 instrument (Spectral Evolution, Haverhill, MA, USA) and a leaf clip, which  
484 covered a leaf surface area of ca. 1 cm<sup>2</sup>. We also measured canopy spectral reflectance 1 m above  
485 the canopy by replacing the fiber optic probe with a 4° field of view lens. Before measuring each  
486 individual, we referenced light conditions using a Spectralon Diffuse Reflectance Standard placed  
487 directly under the fiber optic. We used R version 3.5 (58) and the *spectrolab* package (Meireles et  
488 al., 2018) to import, resample every 1 nm from 400-2400 nm, and normalize to a unit vector all  
489 raw spectra. Additionally, and for the outdoor potted experiment only, we flew an Unoccupied  
490 Aerial Vehicle (UAV) (DJI Inspire2) on days 13, 33, 48, and 62 of the experiment with a custom  
491 Sentera 6X multispectral camera developed in collaboration with Sentera (Saint Paul, MN). The  
492 camera measures reflectance at wavelengths 690 (±20) nm Full Width at Half Maximum, 720 (±10)  
493 nm, 760 (±10) nm, 900 (±20) nm, 970 (±40) nm and an RGB channel. These wavelengths were  
494 selected as important in Sapes *et al.*, (2022) given VNIR sensor constraints (400-990 nm). Digital  
495 numbers from the multispectral images were transformed to reflectance values by the empirical  
496 line method using reflectance values from known surfaces. We used QGIS (59) and the RGB images  
497 of the UAV to manually trace canopies of each tree avoiding empty spaces in each flight date and  
498 convert them to polygons. Polygons were used to extract reflectance at each wavelength from  
499 each pixel within a canopy. Lastly, we calculated the Re-normalized Difference Vegetation Index  
500 (RDVI) (51) as  $(R_{900}-R_{690})/\sqrt{(R_{900}+R_{690})}$ , which Sapes et al. (2022) showed to be highly

501 sensitive to oak wilt. For each flight we estimated mean and standard deviation RDVI within each  
502 tree canopy.

### 503 Water relations

504 We harvested leaves and measured midday leaf water potential (i.e., xylem tension due to  
505 water deficit) in the lab using a pressure chamber (PMS Instrument Company, Corvallis, OR, USA)  
506 following methods in (60). We used the same leaves to measure volumetric (VWC) and relative  
507 water content (RWC), and percent loss of rehydration capacity (LRC). For each sampled tree, an  
508 additional leaf of each type was collected to measure electrolyte leakage (EL). Declines in both  
509 VWC and RWC and increases in EL have been associated with mortality-inducing stress (34, 35,  
510 43); LRC has been associated with irreversible turgor loss and leaf damage (49), which also  
511 contribute to plant stress and mortality. For the sake of space, we describe methods for these  
512 measurements in Appendix S1.

### 513 Xylem staining

514 At the end of the potted experiment, we destructively sampled stem segments 30 cm  
515 above the inoculation point to assess functional and dysfunctional xylem area in a subset of trees  
516 of each treatment (9 C, 14 D, 14 OW, 22 DxOW) using the active xylem staining method (61)  
517 explained in Appendix S1. The staining was done before and after flushing stems at high pressure  
518 to distinguish area of xylem that was embolized from area filled with tyloses. Conduits filled with  
519 tyloses due to oak wilt remained unstained after flushing. Because a subset of the OW trees were  
520 able to slow down the rate of within-tree colonization, we could split OW trees into symptomatic  
521 and asymptomatic. We used ImageJ (62) to measure the percent functional xylem area before  
522 flushing and the percent clogged xylem area after flushing. Additionally, we divided each cross-  
523 section into 16 sections and counted the number of contiguous obstructed xylem sections to  
524 quantify the degree of localized versus multiple xylem obstruction patterning.

### 525 Statistical analyses

#### 526 *Scaling from leaves to whole plant canopies*

527 Both measured and spectrally predicted physiological values were scaled up to the whole  
528 plant level by calculating weighted averages according to the proportion of leaf types in the  
529 canopy. We performed this upscaling to account for spatial variation in both physiology and  
530 spectral reflectance across leaves and ensure that intra-crown variation was considered.

531 *Physiological and spectral progression of oak wilt and drought stress*

532 In all treatments of the potted experiment, trees with larger stem basal perimeters  
533 developed visible symptoms of stress earlier ( $p < 0.001$ , Appendix S3), likely due to higher  
534 transpiration rates. The effect of stem size on symptom development rates was highest in trees  
535 infected with oak wilt that remained well-watered (OW treatment). As a result, we observed large  
536 variability in symptom development rates (Appendix S3) and physiological decline within  
537 treatments. To isolate the influence of treatments rather than inter-individual variation in size, we  
538 represented time as a function of number of days since the start of visible symptoms (Fig. 2B). This  
539 approach also allowed us to assess physiological state before, and after visible symptoms  
540 appeared. To assess physiological differences among oak wilt, drought, and their combined stress,  
541 we built generalized (GLM) and linear (LM) models (63) with each physiological process (VWC,  
542 RWC, LRC, EL, Water Potential, and Fv/Fm) as response variables and the interaction between  
543 treatment and days since the start of visible symptom appearance as predictors. We used GLMs  
544 when response variables could not be transformed to meet LM assumptions. We also built an  
545 additional model with the proportion of healthy leaves as the response variable to assess whether  
546 treatments differed in the timing and rates of symptom development.

547 To assess whether spectra changed in response to stress, we explored the differences in  
548 leaf or canopy spectra in the potted experiment between control and treated trees for each day  
549 that we also measured canopy reflectance with the multispectral UAV (days 13, 33, 48, 62). As  
550 comparisons of reflectance at each measured wavelength would inflate chances of false positives,  
551 we only compared a subset of wavelengths. Wavelengths were selected with a self-designed  
552 mathematical function (Appendix S4) that used the difference in reflectance from one wavelength  
553 to the next to determine the number of wavelengths (i.e., nanometers) to skip. Thus, if two nearby  
554 wavelengths had similar reflectance, the second wavelength would be skipped to find a farther  
555 wavelength with less similar reflectance. The function also considered a minimum (5 nm) and  
556 maximum (40 nm) distance between candidate wavelengths to constrain the magnitude of the  
557 selective jumps. This procedure reduced the number of selected wavelengths from 2000 to 94  
558 wavelengths while still representing the shape of a plant reflectance spectrum across the 400-  
559 2400 nm range. To further reduce chances of false positives, we only considered differences  
560 between treatments to be significant at p-values lower than 0.01.

561 *Spectral prediction of physiology*

562 We built partial least square regression (PLSR) models (64) to test whether processes of  
563 plant dysfunction such as dehydration, cellular death, and cell content leakage could be detected  
564 from spectral reflectance data. Using the dataset from the outdoor potted experiment, we built  
565 models following a 100-iteration, 10-fold validation approach; each physiological variable (VWC,  
566 RWC, LRC, EL, water potential, Fv/Fm) was a response variable and all wavelengths resampled at 1  
567 nm were predictors. For each physiological model, each iteration randomly divided the data into  
568 10 groups and used 9 groups to train a PLSR model. The iteration of that model was then tested  
569 against the remaining group and its performance was assessed based on root mean square error  
570 of prediction in percentage (RMSEP),  $R^2$ , slope, and bias. We optimized the number of components  
571 of the models based on RMSE. We assessed the overall capacity to predict a given physiological  
572 variable by calculating the median RMSEP and  $R^2$  of the 100 iterations run for each physiological  
573 model. Additionally, we extracted wavelength importance values based on Variable Importance in  
574 Projection (VIP, (65)) for each iteration for a given physiological model and calculated the overall  
575 importance of each wavelength as the median importance across all the iterations. Finally, we  
576 validated each physiological model against the independent Cedar Creek experiment dataset. This  
577 experiment's different location provides a useful setup to test whether spectral models are robust  
578 to differences among sites, experimental conditions, and causes of physiological stress. Each  
579 iteration within each physiological model was validated against the full Cedar Creek dataset. Then,  
580 we assessed the overall predictive accuracy of the models on the independent dataset by  
581 calculating the median RMSEP,  $R^2$ , slope, and bias of all 100 iterations, as above. We considered  
582 physiological models with an RMSEP of 20% or less to be acceptable for predicting physiological  
583 processes.

584 *Pre-visual detection of oak wilt and drought stress*

585 Using the dataset from the outdoor potted experiment, we determined whether  
586 spectrally-predicted physiological processes could detect stress before visible symptom expression  
587 using Bayesian segmented regressions from the package *mcp* (66). These regressions identify  
588 inflection points (i.e., changes in status) and provide their location along the x-axis (days since  
589 visible symptom appearance) with confidence intervals around them. The response variables were  
590 the spectrally predicted physiological variables from PLSR models that showed  $RMSEP \leq 20\%$ ,  
591 including VWC, RWC, LRC, EL, Fv/Fm, and WP. Because we measured leaf spectral reflectance in all  
592 trees at each sampling event, we could use our spectrally predicted physiological models to

593 expand our physiological observations from a few trees per day to all trees across the experiment  
594 at each time point. By doing so, we fully captured the existing variability and minimized  
595 uncertainty around the inflection point. Time was expressed in days since the start of visible  
596 symptom appearance; this allowed us to determine if changes in physiology were occurring before  
597 visible symptoms appeared (day 0). We used the default prior settings where priors are informed  
598 based on data properties (minimum, mean, and maximum values of x and y variables and existing  
599 variation), which ensured good parameter estimates. We iterated each model to achieve  
600 convergence between 3 chains by adjusting the “adapt” parameter until the Gelman-Rubin  
601 convergence metric (Rhat) was close to 1 (66). We extracted inflection points and their confidence  
602 intervals for each treatment and variable to assess which inflection points (i.e., day of onset of  
603 physiological decline) were significantly lower than 0 (day of visible symptom appearance).

#### 604 *Physiological and spectral differentiation of oak wilt and drought stress*

605 To test whether physiological stress mechanisms differed between oak wilt and drought,  
606 we assessed differences in functional xylem patterns among treatments before and after flushing  
607 emboli at the end of the experiment. Additionally, we divided OW trees between visually  
608 symptomatic and asymptomatic to distinguish patterns of early and late oak wilt disease  
609 progression. For each of the three measures, we tested differences in percent of functional xylem  
610 before flushing, percent of occluded xylem after flushing, and number of contiguous occluded  
611 xylem sections after flushing among groups using Wilcoxon rank sum tests to account for non-  
612 normal variance between groups. To test the extent to which OW trees displayed higher within-  
613 canopy physiological variability than D trees as they developed symptoms, we built linear models  
614 using within-canopy SD in RDVI as the response variable and the interaction between treatment  
615 and days since the start of symptom appearance as predictors. DxOW trees were not included in  
616 these models because our hypothesis was specifically targeted to differentiate drought from oak  
617 wilt symptoms.

## 618 Acknowledgements

619 This project was funded by the Minnesota Invasive Terrestrial Plants and Pests Center, the  
620 National Aeronautics and Space Administration (NASA) Biodiversity program (Award number:  
621 80NSSC21K1349), the National Science Foundation (NSF) ASCEND Biology Integration Institute  
622 (DBI: 2021898), and the Cedar Creek Long Term Ecological Research program (DEB:1831944). The  
623 University of Minnesota, including Cedar Creek ESR, lies on the ancestral, traditional, and

624 contemporary Land of the Dakota people. We would like to thank C. Lapadat for helping to plant  
625 trees. Thanks to C. Godoy, D. Sannerud, and A. Villaseñor for assistance in Cedar Creek campaigns.  
626 G.S. thanks W. M. Hammond for funding support to present this research at the 2022 Gordon  
627 Research Conference in Plant Vascular Biology. We also thank S. Kothari, and A. Castillo-Castillo  
628 and anonymous reviewers for their comments in previous versions of this manuscript.

## 629 References

- 630 1. IPBES, “Summary for policymakers of the global assessment report on biodiversity and  
631 ecosystem services” (Zenodo, 2019) <https://doi.org/10.5281/ZENODO.3553579> (June 17,  
632 2023).
- 633 2. IPCC, “Summary for Policymakers. In: Climate Change 2023: Synthesis Report. A Report of  
634 the Intergovernmental Panel on Climate Change. Contribution of Working Groups I, II and III  
635 to the Sixth Assessment Report of the Intergovernmental Panel on Climate Change [Core  
636 Writing Team, H. Lee and J. Romero (eds.)]” (2023).
- 637 3. W. M. Hammond, *et al.*, Global field observations of tree die-off reveal hotter-drought  
638 fingerprint for Earth’s forests. *Nat Commun* **13**, 1761 (2022).
- 639 4. N. G. McDowell, *et al.*, Mechanisms of woody-plant mortality under rising drought, CO<sub>2</sub> and  
640 vapour pressure deficit. *Nature Reviews Earth & Environment* **0123456789**, 41–44 (2022).
- 641 5. A. Findlater, I. I. Bogoch, Human Mobility and the Global Spread of Infectious Diseases: A  
642 Focus on Air Travel. *Trends in Parasitology* **34**, 772–783 (2018).
- 643 6. A. Gonzalez, *et al.*, A global biodiversity observing system to unite monitoring and guide  
644 action. *Nat Ecol Evol* (2023) <https://doi.org/10.1038/s41559-023-02171-0> (September 7,  
645 2023).
- 646 7. J. Cavender-Bares, *et al.*, The hidden value of trees: Quantifying the ecosystem services of  
647 tree lineages and their major threats across the contiguous US. *PLOS Sustain Transform* **1**,  
648 e0000010 (2022).
- 649 8. S. Frankel, J. Juzwik, D. M. Rizzo, “North American Oaks” in *Global Plant Health Assessment*,  
650 1st edition, (International Society of Plant Pathology, 2022), pp. 152–158.
- 651 9. J. Juzwik, D. N. Appel, W. L. MacDonald, S. Burks, Challenges and Successes in Managing Oak  
652 Wilt in the United States. *Plant Disease* **95**, 888–900 (2011).
- 653 10. J. Juzwik, D. N. Appel, “Diseases of trees in the Great Plains: Oak Wilt” in *Diseases of Trees in*  
654 *the Great Plains*, (USDA, Forest Service, Rocky Mountain Forest and Range Station, 2016), pp.  
655 129–133.
- 656 11. B. E. Struckmeyer, C. H. Beckman, J. E. Kuntz, A. J. Riker, Plugging of vessels by tyloses and  
657 gums in wilting oaks. *Phytopathology* **44**, 148–153 (1954).

- 658 12. K. A. Yadeta, B. P. Thomma, The xylem as battleground for plant hosts and vascular wilt  
659 pathogens. *Frontiers in Plant Science* **4**, 1–12 (2013).
- 660 13. B. Fallon, *et al.*, Spectral differentiation of oak wilt from foliar fungal disease and drought is  
661 correlated with physiological changes. *Tree Physiology* **40**, 377–390 (2020).
- 662 14. G. Sapes, *et al.*, Canopy spectral reflectance detects oak wilt at the landscape scale using  
663 phylogenetic discrimination. *Remote Sensing of Environment* **273**, 112961 (2022).
- 664 15. J. Pontius, M. Martin, L. Plourde, R. Hallett, Ash decline assessment in emerald ash borer-  
665 infested regions : A test of tree-level, hyperspectral technologies. *Remote Sensing of*  
666 *Environment* **112**, 2665–2676 (2008).
- 667 16. A. Lausch, *et al.*, Forecasting potential bark beetle outbreaks based on spruce forest vitality  
668 using hyperspectral remote-sensing techniques at different scales. *Forest Ecology and*  
669 *Management* **308**, 76–89 (2013).
- 670 17. R. Ogaya, A. Barbeta, C. Başnou, J. Peñuelas, Satellite data as indicators of tree biomass  
671 growth and forest dieback in a Mediterranean holm oak forest. *Annals of Forest Science* **72**,  
672 135–144 (2015).
- 673 18. P. Asner, *et al.*, A Spectral Mapping Signature for the Rapid Ohia Death (ROD) Pathogen in  
674 Hawaiian Forests. *Remote Sensing* **10**, 1–14 (2018).
- 675 19. P. J. Zarco-Tejada, *et al.*, Previsual symptoms of *Xylella fastidiosa* infection revealed in  
676 spectral plant-trait alterations. *Nature Plants* **4**, 432–439 (2018).
- 677 20. M.-D. Iordache, V. Mantas, E. Baltazar, K. Pauly, N. Lewyckyj, A Machine Learning Approach  
678 to Detecting Pine Wilt Disease Using Airborne Spectral Imagery. *Remote Sensing* **12**, 2280  
679 (2020).
- 680 21. A. Hornero, *et al.*, Modelling hyperspectral- and thermal-based plant traits for the early  
681 detection of *Phytophthora*-induced symptoms in oak decline. *Remote Sensing of*  
682 *Environment* **263**, 112570 (2021).
- 683 22. L. Cotrozzi, Spectroscopic detection of forest diseases: a review (1970–2020). *J. For. Res.* **33**,  
684 21–38 (2022).
- 685 23. J. A. Guzmán Q., *et al.*, “Mapping oak wilt disease using phenological observations from  
686 space” (*Ecology*, 2023) <https://doi.org/10.1101/2023.05.25.542318> (June 25, 2023).
- 687 24. C. Bhuiyan, R. P. Singh, F. N. Kogan, Monitoring drought dynamics in the Aravalli region  
688 (India) using different indices based on ground and remote sensing data. *International*  
689 *Journal of Applied Earth Observation and Geoinformation* **8**, 289–302 (2006).
- 690 25. L. Cotrozzi, *et al.*, Using foliar spectral properties to assess the effects of drought on plant  
691 water potential. *Tree Physiology* **37**, 1582–1591 (2017).

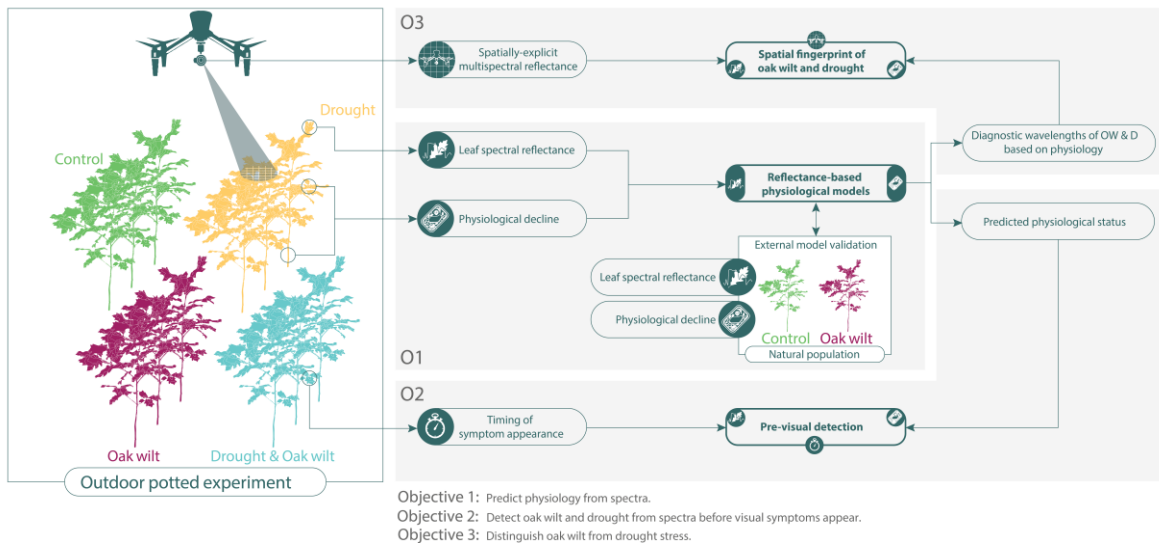
- 692 26. P. D. Dao, Y. He, C. Proctor, Plant drought impact detection using ultra-high spatial resolution  
693 hyperspectral images and machine learning. *International Journal of Applied Earth*  
694 *Observation and Geoinformation* **102**, 102364 (2021).
- 695 27. W. Jiao, L. Wang, M. F. McCabe, Multi-sensor remote sensing for drought characterization:  
696 current status, opportunities and a roadmap for the future. *Remote Sensing of Environment*  
697 **256**, 112313 (2021).
- 698 28. D. Marusig, *et al.*, Correlation of Field-Measured and Remotely Sensed Plant Water Status as  
699 a Tool to Monitor the Risk of Drought-Induced Forest Decline. *Forests* **11**, 77 (2020).
- 700 29. J. Penuelas, I. Filella, C. Biel, L. Serrano, R. Save, The reflectance at the 950-970 nm region as  
701 an indicator of plant water status. *International Journal of Remote Sensing* (1993)  
702 <https://doi.org/10.1080/01431169308954010>.
- 703 30. P. J. Zarco-Tejada, *et al.*, Divergent abiotic spectral pathways unravel pathogen stress signals  
704 across species. *Nat Commun* **12**, 6088 (2021).
- 705 31. E. Weingarten, *et al.*, Early detection of a tree pathogen using airborne remote sensing.  
706 *Ecological Applications* **32** (2022).
- 707 32. C. R. Guadagno, *et al.*, Dead or alive? Using membrane failure and chlorophyll fluorescence  
708 to predict mortality from drought. *Plant Physiology* **175**, 223–234 (2017).
- 709 33. J. Martinez-Vilalta, W. R. L. Anderegg, G. Sapes, A. Sala, Greater focus on water pools may  
710 improve our ability to understand and anticipate drought-induced mortality in plants. *New*  
711 *Phytologist* **223**, 22–32 (2019).
- 712 34. G. Sapes, *et al.*, Plant water content integrates hydraulics and carbon depletion to predict  
713 drought-induced seedling mortality. *Tree Physiology* **39**, 1300–1312 (2019).
- 714 35. M. Mantova, P. E. Menezes-Silva, E. Badel, H. Cochard, J. M. Torres-Ruiz, The interplay of  
715 hydraulic failure and cell vitality explains tree capacity to recover from drought. *Physiologia*  
716 *Plantarum*, ppl.13331 (2021).
- 717 36. S. P. Serbin, *et al.*, Remotely estimating photosynthetic capacity, and its response to  
718 temperature, in vegetation canopies using imaging spectroscopy. *Remote Sensing of*  
719 *Environment* **167**, 78–87 (2015).
- 720 37. A. Onofri, P. Benincasa, M. B. Mesgaran, C. Ritz, Hydrothermal-time-to-event models for  
721 seed germination. *European Journal of Agronomy* **101**, 129–139 (2018).
- 722 38. H. Lambers, F. S. Chapin III, T. L. Pons, *Plant physiological ecology*, 2nd Ed. (2009).
- 723 39. O. L. Lange, R. L. Sch, E.-D. Schulze, L. Kappen, Responses of stomata to changes in humidity.  
724 *Planta* **100**, 76–86 (1971).

- 725 40. H. A. Snyman, W. L. J. Van Rensburg, W. D. Venter, Transpiration and water-use efficiency in  
726 response to water stress in *Themeda triandra* and *Eragrostis lehmanniana*. *South African*  
727 *Journal of Botany* **63**, 55–59 (1997).
- 728 41. W. M. Hammond, *et al.*, Dead or dying? Quantifying the point of no return from hydraulic  
729 failure in drought-induced tree mortality. *New Phytologist* **223**, 1834–1843 (2019).
- 730 42. M. Mantova, S. Herbette, H. Cochard, J. M. Torres-Ruiz, Hydraulic failure and tree mortality:  
731 from correlation to causation. *Trends in Plant Science* **27**, 335–345 (2022).
- 732 43. G. Sapes, A. Sala, Relative water content consistently predicts drought mortality risk in  
733 seedling populations with different morphology, physiology and times to death. *Plant, Cell &*  
734 *Environment* **44**, 3322–3335 (2021).
- 735 44. G. L. Beier, B. W. Held, C. P. Giblin, J. Cavender-Bares, R. A. Blanchette, American elm  
736 cultivars: Variation in compartmentalization of infection by *Ophiostoma novo-ulmi* and its  
737 effects on hydraulic conductivity. *Forest Pathology* **47**, e12369 (2017).
- 738 45. J. Oliva, J. Stenlid, J. Martinez-Vilalta, The effect of fungal pathogens on the water and carbon  
739 economy of trees: implications for drought-induced mortality. *New Phytologist* **203**, 1028–  
740 1035 (2014).
- 741 46. K. R. Hargrave, K. J. Kolb, F. W. Ewers, S. D. Davis, Conduit Diameter and Drought-Induced  
742 Embolism in *Salvia-Mellifera* Greene (Labiatae). *New Phytologist* **126**, 695–705 (1994).
- 743 47. P. Fu, K. Meacham-Hensold, K. Guan, J. Wu, C. Bernacchi, Estimating photosynthetic traits  
744 from reflectance spectra: A synthesis of spectral indices, numerical inversion, and partial  
745 least square regression. *Plant Cell Environ* **43**, 1241–1258 (2020).
- 746 48. P. Trifilò, E. Abate, F. Petruzzellis, M. Azzarà, A. Nardini, Critical water contents at leaf, stem  
747 and root level leading to irreversible drought-induced damage in two woody and one  
748 herbaceous species. *Plant Cell & Environment* **46**, 119–132 (2023).
- 749 49. S. Trueba, *et al.*, Thresholds for leaf damage due to dehydration: declines of hydraulic  
750 function, stomatal conductance and cellular integrity precede those for photochemistry.  
751 *New Phytologist* **223**, 134–149 (2019).
- 752 50. J. Juzwik, J. O'Brien, C. Evenson, P. Castillo, G. Mahal, Controlling Spread of the Oak Wilt  
753 Pathogen (*Ceratocystis fagacearum*) in a Minnesota Urban Forest Park Reserve. *AUF* **36**, 171–  
754 178 (2010).
- 755 51. J.-L. Roujean, F.-M. Breon, Estimating PAR absorbed by vegetation from bidirectional  
756 reflectance measurements. *Remote Sensing of Environment* **51**, 375–384 (1995).
- 757 52. J. Juzwik, An oak wilt primer. *International Oaks* **11**, 14–20 (2000).
- 758 53. A. Galieni, *et al.*, Past and Future of Plant Stress Detection: An Overview From Remote  
759 Sensing to Positron Emission Tomography. *Front. Plant Sci.* **11**, 609155 (2021).

- 760 54. J. Cavender-Bares, *et al.*, Integrating remote sensing with ecology and evolution to advance  
761 biodiversity conservation. *Nat Ecol Evol* **6**, 506–519 (2022).
- 762 55. H. Hartmann, *et al.*, Research frontiers for improving our understanding of drought-induced  
763 tree and forest mortality. *New Phytologist* **218**, 15–28 (2018).
- 764 56. N. Garcia-Forner, A. Sala, C. Biel, R. Savé, J. Martínez-Vilalta, Individual traits as determinants  
765 of time to death under extreme drought in *Pinus sylvestris* L. *Tree Physiology* **36**, 1196–1209  
766 (2016).
- 767 57. J. Cavender-Bares, F. A. Bazzaz, Changes in drought response strategies with ontogeny in  
768 *Quercus rubra*: implications for scaling from seedlings to mature trees. *Oecologia* **124**, 8–18  
769 (2000).
- 770 58. R Core Team, R: A language and environment for statistical computing (2020).
- 771 59. QGIS Development Team, QGIS Geographic Information System. Open Source Geospatial  
772 Foundation Project. (2009).
- 773 60. M. Kaufmann, Evaluation of the Pressure Chamber Technique for Estimating Plant Water  
774 Potential of Forest Tree Species. *Forest Science* **14**, 369–374 (1968).
- 775 61. A. L. Jacobsen, R. B. Pratt, F. W. Ewers, S. D. Davis, Cavitation Resistance among 26 Chaparral  
776 Species of Southern California. *Ecological Monographs* **77**, 99–115 (2007).
- 777 62. C. A. Schneider, W. S. Rasband, K. W. Eliceiri, NIH Image to ImageJ: 25 years of image  
778 analysis. *Nat Methods* **9**, 671–675 (2012).
- 779 63. K. V. Mardia, J. T. Kent, J. M. Bibby, *Multivariate Analysis* (Academic Press, 1979).
- 780 64. S. Wold, M. Sjöström, L. Eriksson, PLS-regression: a basic tool of chemometrics.  
781 *Chemometrics and Intelligent Laboratory Systems* **58**, 109–130 (2001).
- 782 65. M. Kuhn, Building Predictive Models in R Using the caret Package. *Journal of Statistical*  
783 *Software* **28** (2008).
- 784 66. J. K. Lindeløv, “mcp: An R Package for Regression With Multiple Change Points” (Open  
785 Science Framework, 2020) <https://doi.org/10.31219/osf.io/fzqxv> (March 26, 2023).
- 786

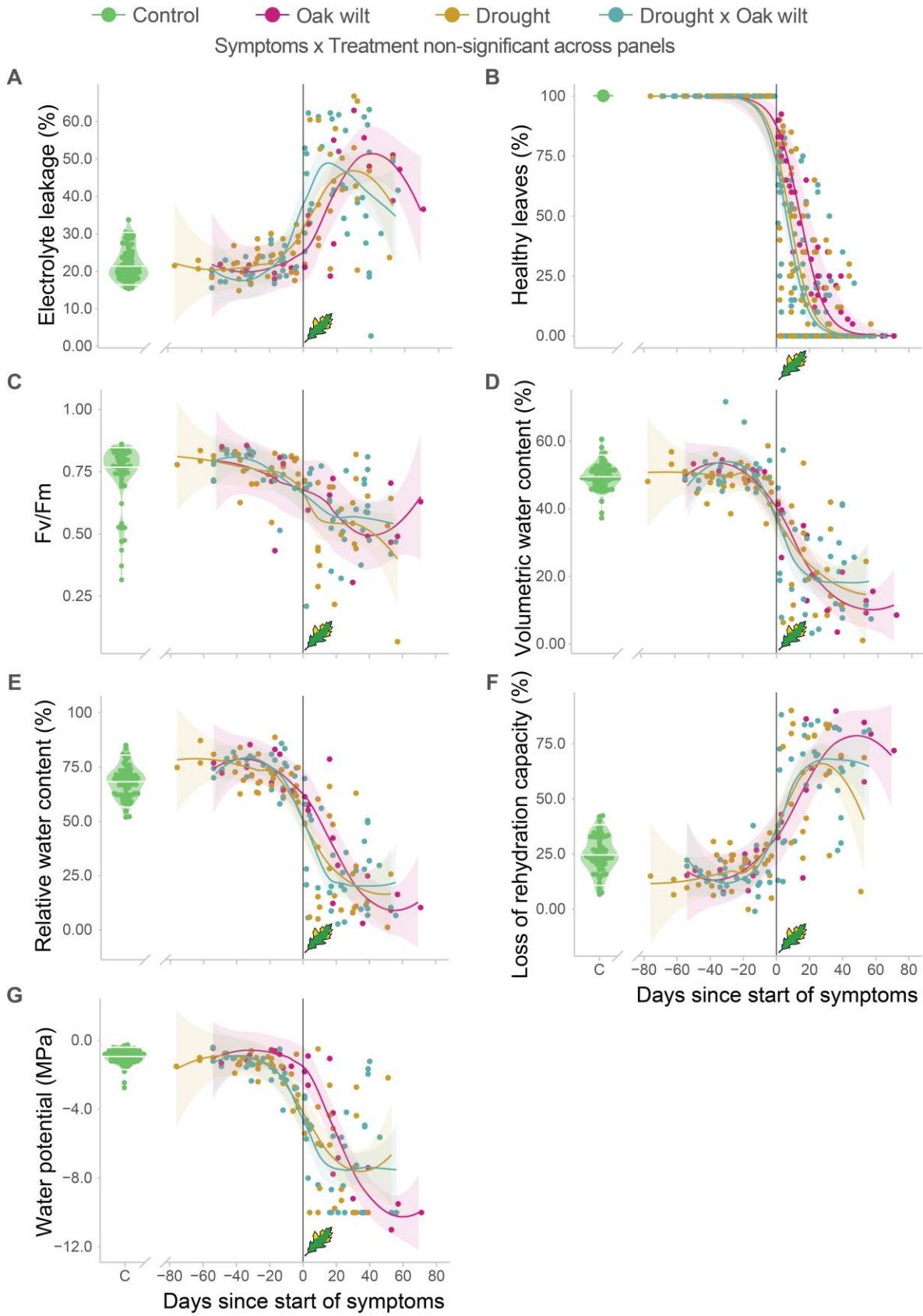
## 787 Figures

788

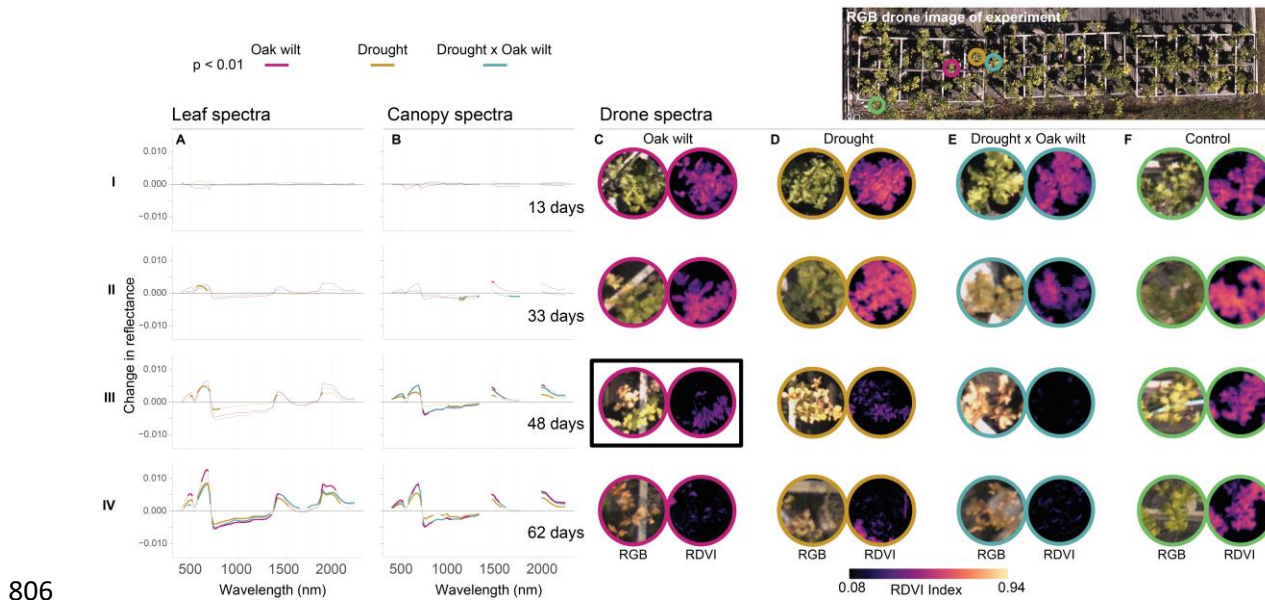


789

790 **Fig 1:** Logic schematic of the experimental design, questions, and methodological approach. The  
 791 panel on the left depicts treatment groups and methods of spectral imaging, both at the canopy  
 792 and the leaf level. Each of the gray boxes indicates the approach taken to answer the three main  
 793 objectives which are: (O1) Predict physiology from spectra, (O2) detect oak wilt and drought from  
 794 spectra before visual symptoms appear, and (O3) distinguish oak wilt from drought stress.



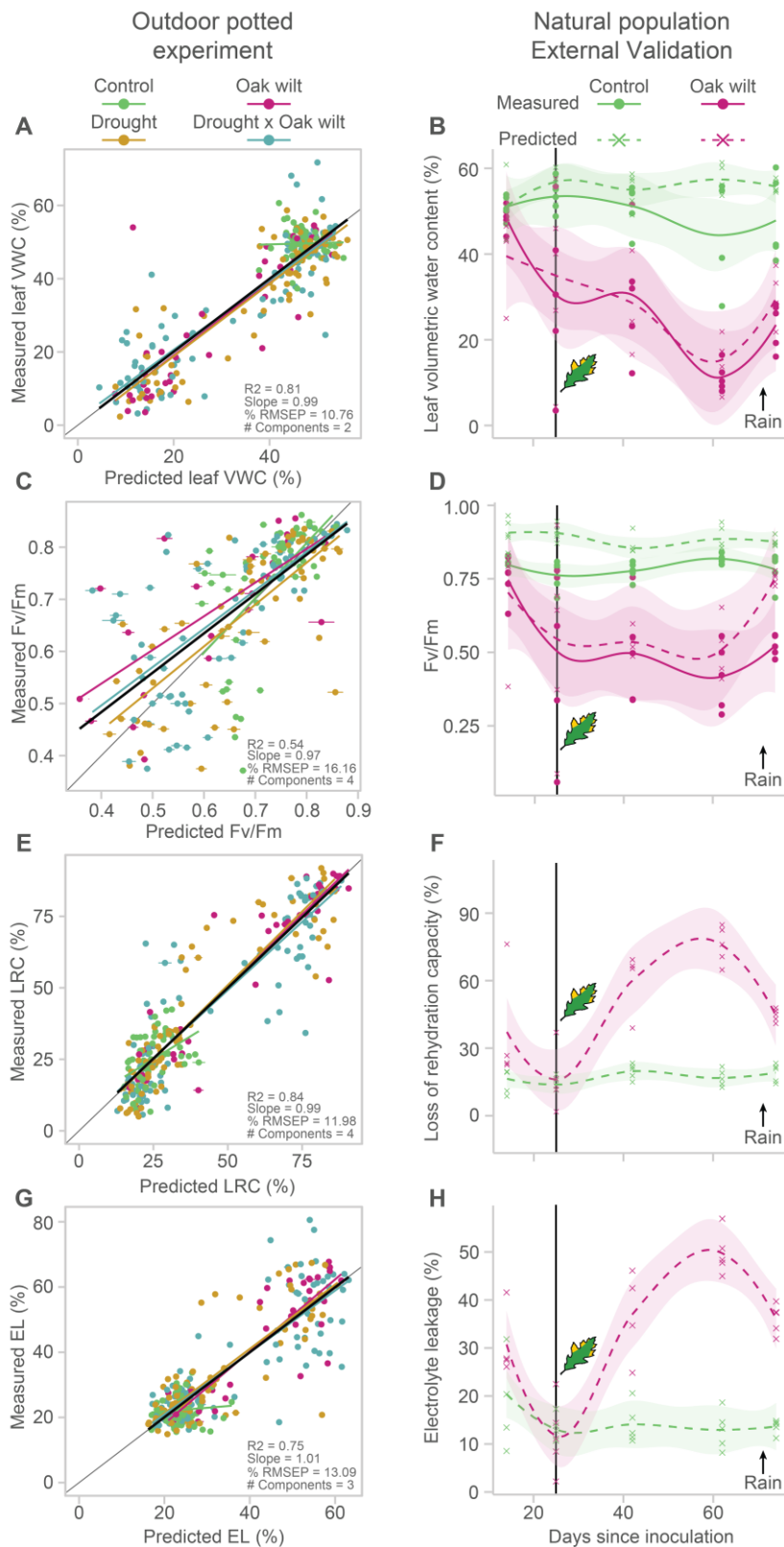
796 **Fig 2:** Progression of physiological symptoms in oak wilt (OW), drought (D), and drought plus oak  
 797 wilt (DxOW) treatments. The violin plots in green indicate the median and range of physiological  
 798 status observed in the control group (C) across the duration of the experiment. The black vertical  
 799 line and leaf icon at day 0 indicate the start of visual symptoms. Leaves not counted as healthy  
 800 (i.e., wilted, brown edges, or dry) are considered visually symptomatic, as indicated in the decline  
 801 in healthy leaves (B). Electrolyte leakage (A) and loss of rehydration capacity (F) increase before  
 802 visual symptoms appear, whereas Fv/Fm (C), relative water content (E), volumetric water content  
 803 (D), and water potential (G) decline before the start of symptoms. All panels show statistically  
 804 significant effects of days since start of symptoms on the response variables, but we did not detect  
 805 significant differences in slopes among treatments.



806

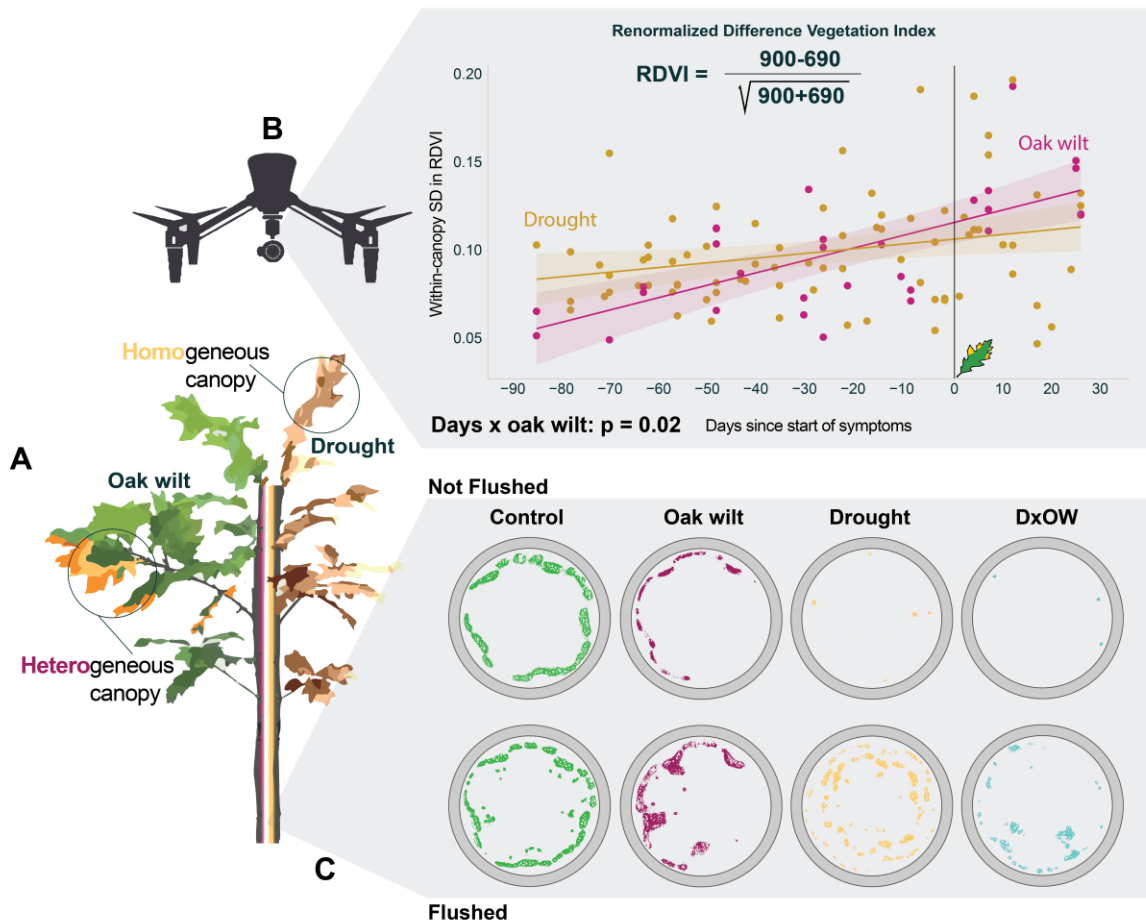
807 **Fig 3:** Repeated measurements of leaf- (A), canopy- (B), and UAV-measured spectra (C-F) over the  
 808 course of stress progression allowed identification of wavelengths indicative of oak wilt (OW) and  
 809 drought (D) stress at different stages of physiological decline. The heterogenous physiological  
 810 decline within canopies of oak wilt trees during early stages of infection can be clearly observed in  
 811 the UAV-measured Re-normalized Difference Vegetation Index (RDVI) images at 48 days since the  
 812 start of the experiment (black box in C III), but decline was already noticeable at 33 days (black box  
 813 in C III). 33 days corresponds to the date in which visible symptoms of stress appeared for the oak  
 814 wilt-infected tree shown in the outlined box. Columns A and B show the difference in normalized  
 815 reflectance between control and treated trees at each date (13, 33, 48, and 62 days) since the

816 start of the experiment. Bolded line segments in columns A and B show wavelengths with  
 817 significant ( $p < 0.01$ ) changes over time.



818

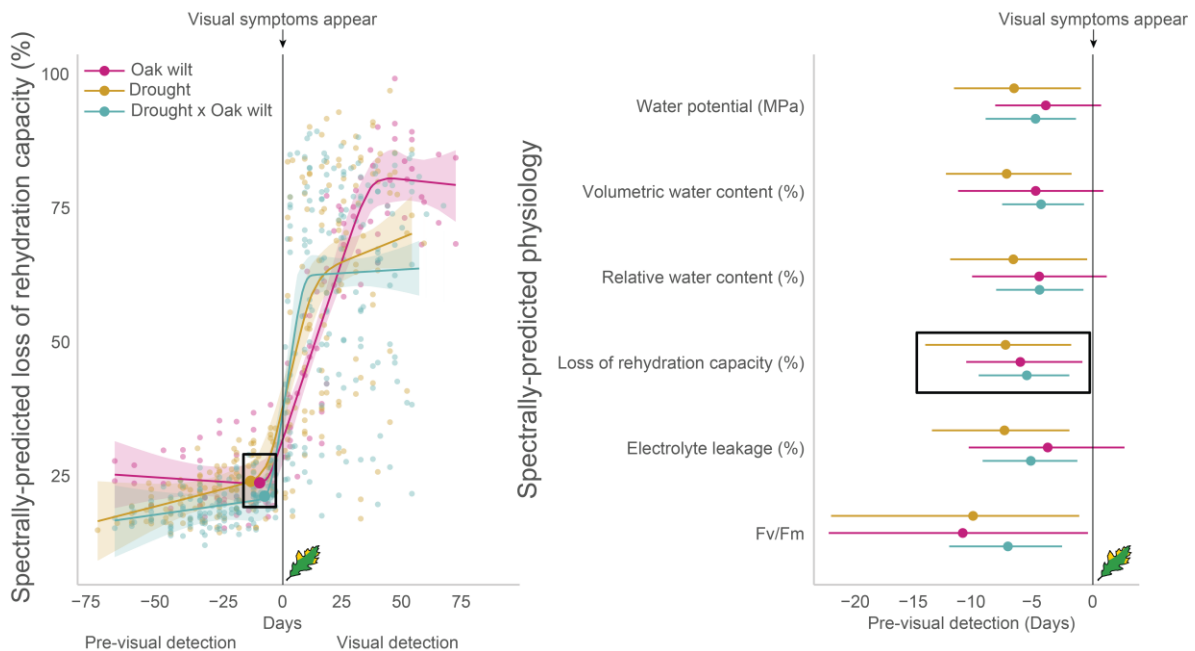
819 **Fig 4:** Predictions of physiology from spectral reflectance using PLSR models. On the left panel  
 820 (A,C,E,G) are measured vs. predicted plots from the models. The thin, gray line indicates a 1:1 fit.  
 821 The black line indicates the overall model fit across treatments. All other lines represent the  
 822 overall model fit within each treatment and are colored according to their treatment  
 823 (control=green, oak wilt=purple, drought=gold, drought X oak wilt=blue). On the right panel (B,D,  
 824 F, H), the models were validated using an external dataset from the Cedar Creek natural  
 825 population field experiment. Circles indicate the measured values, and crosses indicate the  
 826 predicted values. A leaf icon and black vertical line indicate the date of visual symptoms detected.  
 827 An arrow indicates the date of a rain event that led to a recovery of function.  
 828



829

830 **Fig 5:** Oak wilt spreads through the stem vascular system, blocking conduits and causing  
 831 dysfunction in localized areas of the wood, as indicated by a lack of dye in areas of the stem cross  
 832 sections while other areas remain functional (shown as red colored areas, panel C, not flushed). In  
 833 contrast, drought reduces water flow through the vascular system as a function of conduit size

834 because wide vessels are often more vulnerable to bubble formation and cavitation. Drought thus  
 835 generates a non-localized pattern of loss in xylem function (yellow coloring shows the small  
 836 number of functional xylem vessels under drought stress, and blue coloring shows the still smaller  
 837 number of functional vessels under drought and oak wilt stress, panel C, not flushed). Drought-  
 838 induced air bubbles can be flushed out with high pressure dye-infused water while blockages from  
 839 oak wilt cannot be flushed (panel C, flushed). At early stages of infection, the localized dysfunction  
 840 caused by oak wilt in the xylem leads to localized physiological decline in the foliar canopies. This is  
 841 because some branches and the leaves they support are connected to blocked vessels while most  
 842 remain connected to functional ones. Oak wilt-infected canopies are thus more physiologically  
 843 heterogeneous than drought-stressed canopies (panel A). This heterogeneity can be spatially  
 844 detected by measuring within-canopy variability using UAVs and spectral indexes associated with  
 845 physiological decline, such as the Re-normalized Difference Vegetation Index (RDVI, panel B).  
 846



847

848 **Fig 6:** Left panel: Bayesian segmented regressions (left panel) identified inflection points (black  
 849 box) corresponding to the day in which spectrally-predicted physiological decline (e.g., loss of  
 850 rehydration capacity associated to cell damage) started. Day 0 of the X axis represents the day in  
 851 which visual symptoms appeared. Negative and positive values correspond to days prior and after  
 852 the day of symptom appearance, respectively. If the inflection point occurs before day 0, the  
 853 spectrally-predicted physiological process can detect stress before visual symptoms appear. Right

854 panel: Inflection points for each spectrally-predicted physiological process and stress type. Lines  
855 represent confidence intervals around the predicted onset of physiological symptoms. All  
856 spectrally-predicted physiological processes detected drought stress or combined drought and oak  
857 wilt stress prior to the appearance of visual symptoms (i.e., confidence intervals do not overlap  
858 with day 0, vertical black line). However, only spectrally-predicted loss of rehydration capacity and  
859 Fv/Fm (related to photosynthetic activity) detected stress associated with oak wilt before visual  
860 symptoms appeared. Loss of rehydration capacity detected oak wilt between 11 to 2 days before  
861 visual symptoms appeared (average of 7) while Fv/Fm detected oak wilt between 26 to 1 days  
862 before visual symptoms appeared. Physiological changes associated with oak wilt did not always  
863 occur before visual symptoms appeared (confidence intervals overlap with the 0 days) but were  
864 still detectable as early as 3 days after visual symptoms appeared.